JOHANNES KEPLER
UNIVERSITY LINZ

Submitted by
Katarina Gugujonović

Submitted at
Institute of Physical Chemistry and Linzer Institute of Organic Solar Cells

Supervisor
Assoc. Prof. DI Dr. Markus Scharber

January 2019

AN ALTERNATIVE NON-FULLERENE ACCEPTOR FOR ORGANIC SOLAR CELLS

Bachelor Thesis

to obtain the academic degree of

Bachelor of Science

in the bachelor's program

Technical Chemistry

JOHANNES KEPLER UNIVERSITY LINZ
Altenberger Str. 69
4040 Linz, Austria
www.jku.at
DVR 0093696

JOHANNES KEPLER
UNIVERSITY LINZ

Statutory declaration

I hereby declare that the thesis submitted is my own unaided work, that I have not used other than the sources indicated, and that all direct and indirect sources are acknowledged as references.
This printed thesis is identical with the electronic version submitted.

Linz, 11 February 2019

Acknowledgement

First of all, I would like to thank o.Univ. Prof. Mag. Dr. DDr. H.c. Niyazi Serdar Sarıçiftçi for introducing me to the Linzer Institute for Organic Solar Cells and for giving me the opportunity to work on this special topic and together with fantastic humans.
My biggest thanks go to my supervisor Assoc. Prof. DI Dr. Markus Scharber for his great support and for all the time he spent answering my questions, leading me through this highly interesting topic and of course for the kind conversations.
Also a big thank you to the LIOS group for the warm welcome and their help in so many questions. Especially I would like to thank Patrick Denk for introducing me to the preparation techniques of organic solar cells and Bekele Teklemariam MSc for his encouraging words.
Thanks Anna Reitinger for your time and effort while proofreading this work.
Finally I would like to thank my family and friends for bolstering me and showing their interest for my research.

Abstract

$PC_{60}BM$ (Phenyl-C61-butyricacidmethylester) is a fullerene derivate and the most commonly used acceptor in organic photovoltaics. It became popular after the photoelectric characteristics of Buckminster fullerenes had been discovered in 1992. A side chain has been added to increase the solubility of the material in aromatic solvents and in further consequence to enable the usage of simple application techniques. A pleasant side aspect is that using a solution based on chlorobenzene often leads to a more optimized morphology of the thin semiconductor films. Nevertheless, the thermal instability of the material combined with a donor molecule in a bulk makes the solar cell less efficient over a certain time. When illuminating the solar cell, the material gets heated, which leads to particularly pronounced separation of donor and acceptor, so that the formed clusters inhibit the charge generation in the active layer. The high production costs, limited spectral absorption and a wide band gap of 2 eV accentuate that $PC_{60}BM$ is not the best acceptor candidate. In this thesis an alternative non-fullerene acceptor, called EH-IDTBR (5,5'-[(4,9-Dihydro-4,4,9,9-tetrakis(2-ethylhexyl)-s-indaceno[1,2-b:5,6-b']dithiophene-2,7-diyl)bis(2,1,3-benzothiadiazole-7,4-diylmethylidyne)]-bis[3-ethyl-2-thioxo-4-thiazolidinone]), is investigated and compared to $PC_{60}BM$. The planarity of the molecule core has the effect of shifting the absorption spectra to longer wavelengths compared to $PC_{60}BM$, which leads to a higher probability of charge carrier generation. Another impact is the formation of clusters in the length scales that are ideal for charge transport. With this material a power conversion efficiency of 6.4 % has been achieved in P3HT solar cells, which is the highest reported value till now. Although P3HT was the best known and most prominent donor material for some time, much higher efficiencies with other optimized polymers are possible. The possibility of applying the films at ambient conditions is an additional reason for using PBDTTT-EFT (Poly[4,8-bis(5-(2-ethylhexyl)thiophen-2-yl)benzo[1,2-b;4,5-b']dithiophene-2,6-diyl-alt-(4-(2-ethylhexyl)-3-fluorothieno[3,4-b]thiophene)-2-carboxylate-2-6-diyl)]) as donor for the active layer in the solar cells. For the comparison of the two acceptor materials the current-voltage characteristics, the external quantum efficiency and the electroluminescence quantum efficiency are measured. The photoluminescence and the electroluminescence are shown as a function of the applied voltage to show the influence on the charge transfer state in organic solar cells. In addition, the influence of the acceptor on the charge transfer state is illustrated and discussed.

Table of Contents

1. Introduction

Organic solar cells are a promising class of photovoltaic devices. The photoactive layer that is sandwiched between two electrodes can be applied on transparent and flexible substrates. Semiconductors with electron donating and electron accepting properties are mixed on a nanometer scale to achieve efficient conversion of photons into electron hole pairs. For a long time, fullerene derivates mixed with a conjugated polymer have been used as absorber layers in organic solar cells [1]. It is well established today that the use of fullerene derivates limit the power conversion efficiency of these devices [2]. Therefore, so-called non-fullerene acceptors have been developed to overcome these limitations. In this thesis a blend of polymer and non-fullerene acceptor is studied. Solar cells with two different acceptors are prepared and characterized. The role of a charge transfer state and the radiative recombination of electron-hole pairs are the focus to this study as both are of critical importance for the efficiency of organic solar cells [3].

2. Brief History

It was in 1838, when Becquerel discovered a light-electricity conversion while he was doing experiments with electrodes in electrolytes [4]. In 1883, Fritts described the Se/Pt junction of the first functional photovoltaic device [5]. In 1905, Einstein published a paper, in which he gave a mathematical description of the photovoltaic effect when photons are absorbed. Therefore he built the fundamental base for understanding the absorption processes in solar cells [6]. The history of organic solar cells with conjugated polymers started in the early 20th century when Volmer studied the photoconductivity of the compound anthracene [7]. In 1942, Carlson was the first who mentioned anthracene as a possible photoreceptor in imaging systems, which led to an increased research into photoconductivity [8]. Bell Laborites discovered a photovoltage while illuminating silicon-based p-n-junction diodes with ambient light. Within one year they developed the first inorganic solar cell, that reached a power conversion efficiency of 6 %. Today the efficiency of silicon solar cells is around 24 % [4]. After discovering of several aromatic semi-conductive compounds, Inokuchi firstly entrenched the term “organic semiconductors” in 1954 [9]. In the 1960s was discovered that many common dyes, like perylene, have photoconductive properties [10]. Inspired by photosynthesis, Tang and Albrecht investigated the photovoltaic effect of chlorophyll solar cells [11]. Although organic polymers were known for their insulating properties, the fundamental research of Shirakawa and coworkers showed that the opposite could be possible. With their synthesis of halogenated polyacetylene derivates they produced the first conductive organic polymer in 1977 [12]. After several years elapsed without considerable publications, the number of papers of non-dye-sensitized organic solar cells increased exponentially since 1985 [13]. By optimizing absorption materials and design by Tang, the first organic solar cell with a power conversion efficiency of 1 % was demonstrated in 1986 [14]. Sarıçiftçi and coworkers discovered the photoinduced charge transfer from a conducting polymer to Buckminster fullerene in 1992 [15]. From that time on the idea of combining a donor and an acceptor material in the photoactive layer was born.

3. Theory

Photovoltaics is a technology to convert light into direct current electrical energy. Used materials are semiconductors, where electrons can be excited from the valence band to the conduction band by exceeding a certain threshold energy, called band gap [4]. As a consequence, a so-called hole remains in the valence band. The required energy can be generated by absorbing a photon, which must have at least the energy of $\varepsilon_G = h \cdot \nu$. **Figure 1** illustrates this schematically. Photons with lower energy are not absorbed, the excess energy of high energy photons is dissipated in small steps by generating phonons, until the excited electron reaches the lower edge of the conduction band of the semiconductor. The electron has a life time up to 10^{-3} s, in that time it must be extracted from the semiconductor material. Otherwise, charge carriers will return to the ground state by emitting a large number of phonons or a photon and will not contribute to the photocurrent. Each absorbed photon can only generate one electron hole pair. The smaller the band gap, the larger the losses when high energy photons are absorbed and the smaller the energy stored in each electron hole pair [16]. Consequently, the maximum efficiency of an ideal solar cell when exposed to extraterrestrial solar radiation can be estimated at around 31 % by assuming perfect absorption of the photons, infinite charge carrier mobility and that only radiative recombination is allowed [17]. For the AM1.5 spectra the limit is 33.3 %. The ideal band gap is in the range of 1.0 – 1.5 eV. In silicon solar cells the partition of electron and hole is much faster compared to organic photovoltaics [1].

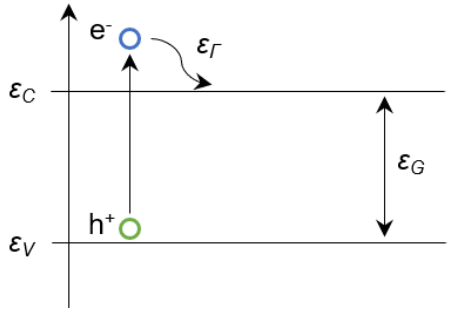

Figure 1 Excitation of an electron from the valence band to the conduction band by absorbing a photon. ε_C… energy level of the conduction band in a semiconductor, ε_V… energy level of the valence band in a semiconductor, ε_Γ… excessive energy from the absorbed photon, ε_G… band gap of the semiconductor.

Organic semiconductors are defined as conjugated molecules in which sp^2-hybridized atom orbitals in the main chain of the molecule overlap and form the bonding molecular orbital σ and the antibonding molecular orbital σ^*. The remaining p_z orbitals, that overlap less, form the bonding and antibonding molecular orbitals π and π^*. At the ground-state the π-orbital (HOMO) is filled with two electrons with antiparallel spins whereas the π^*-orbital (LUMO) is empty [18]. Due to no further energetic states in between this section is called the forbidden zone. The binding energy of an excited electron-hole-pair, the so called exciton, in an organic semiconductor can be estimated by Coulomb's law by assuming a low relative dielectric constant at 3.5 A s V^{-1} m^{-1} [19] and the distance of electron and hole at 1 nm. The result is a binding energy of 0.4 eV, which is much higher than the available thermal energy at room temperature $k_b \cdot T$ and therefore a separation is not very likely. By combining a donor and an acceptor material as photoactive layer, a dissociation of the exciton is possible. The

requirements for these materials are that the electron transfer from donor to acceptor and the hole transfer from acceptor to donor must be energetic facilitated as illustrated in **Figure 2**. In addition, the difference of the two LUMO states |LUMO(D) – LUMO(A)|, as well as |HOMO(D) – HOMO(A)|, must be larger than the binding energy of the exciton to enable a fast charge transfer due to the relatively short life time of an exciton. The effective wavelength results from ε_G(D) - ΔLUMO [20]. The HOMO level of the donor molecule is in a linear relation to the open circuit voltage and to the oxidation potential [21]. In organic bulk heterojunction solar cells, emissions at low energy values are observed, suggesting that a charge transfer complex, also called bound polaron pairs, is formed. It is a state between exciton dissociation and free charge generation localized on the donor-acceptor interface and plays an important role in organic solar cells. The maximum value of the open circuit voltage is determined by the energetic position of the CT state. Charge generation and recombination through this state are one of the efficiency limiting factors in bulk heterojunction cells [3].

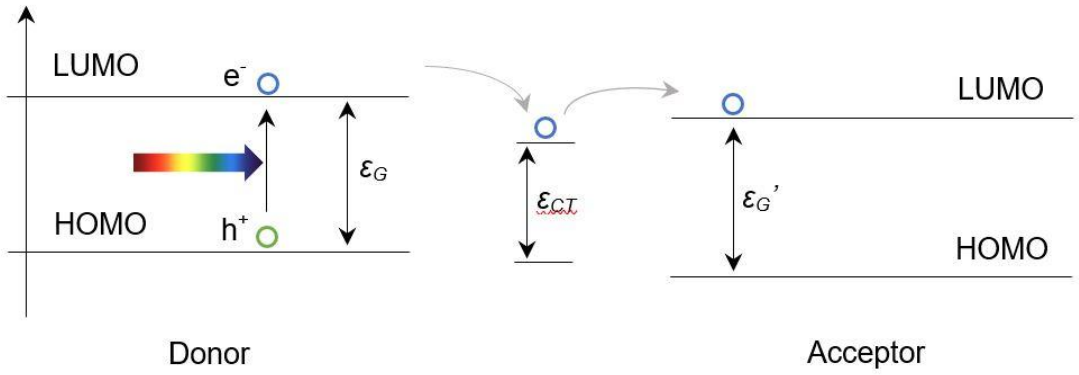

Figure 2 Schematic diagram of the donor-acceptor levels in an OPV.
ε_G… band gap of the donor material, ε_{CT}… *band gap of the charge transfer state,* $\varepsilon_{G'}$… band gap of the acceptor material.

The process of generating electrons and holes discussed before can also happen in reverse, when an electron and a hole combines in a process called recombination. Beside the radiative recombination, in which photons are emitted upon recombination, also several nonradiative recombination mechanisms are active in organic solar cells. In one of them the energy set free by the recombination of an electron hole pair is absorbed by a free carrier, either an electron or a hole. In further consequence this excited carrier gives the excess energy to the lattice by entering the lower edge of the conduction band. In this so-called Auger recombination two electrons and one hole or two holes and one electron participate and therefore Auger recombination is more likely for highly doped materials. Other recombination losses can occur when impurities acting as recombination centers are present in the lattice. Several kinds of impurities can offer electronic states that are located between the valence band and the conduction band. The closer these states are located to the middle of the forbidden zone, the higher is the probability of nonradiative recombination. In real solar cells recombination via impurities is the predominant recombination process. A similar process takes place at the surface of a semiconductor, where neighboring atoms are not available and impurities like H_2O or O_2 can be absorbed. This leads to a continuous distribution of electron state in the forbidden zone and therefore recombination is much more likely [16].

An exciton needs to be generated near the donor acceptor interface of an organic solar cell, since its diffusion length is typically 5-10 nm [22]. Of course, applying such thin layers can be very difficult, never mind that the ability of absorption and therefore the generation of current decreases by reducing the layer thickness to that scale [23]. Another possibility would be to arrange the donor and acceptor species in a way that all incoming photons can be absorbed less than a diffusion length away from the interface, which is commonly done. On the one hand, a completely mixed donor-acceptor blend, which is shown in **Figure 3 (a)**, will lead to an almost perfect charge generation. On the other hand, the charge carrier transport will be inhibited due to high recombination losses. For the morphology in **Figure 3 (b)** the charge transport will be ideal because there are no barriers for the charge carriers after generation on the way to the electrode. Nevertheless, the charge generation can only occur on the interface of the two materials and therefore a small interface area leads to poor charge carrier generation. An ideal arrangement with highly structured domains is illustrated in **Figure 3 (c)**. These domains with a width of two times the diffusion length of the exciton will ensure efficient charge generation and optimal charge transport. Due to the difficult processing of this ideal morphology a self-organized phase separation during the formation of the active layer is preferred. This particular donor-acceptor separation based on the finite miscibility of the materials is represented in **Figure 3 (d)** [20].

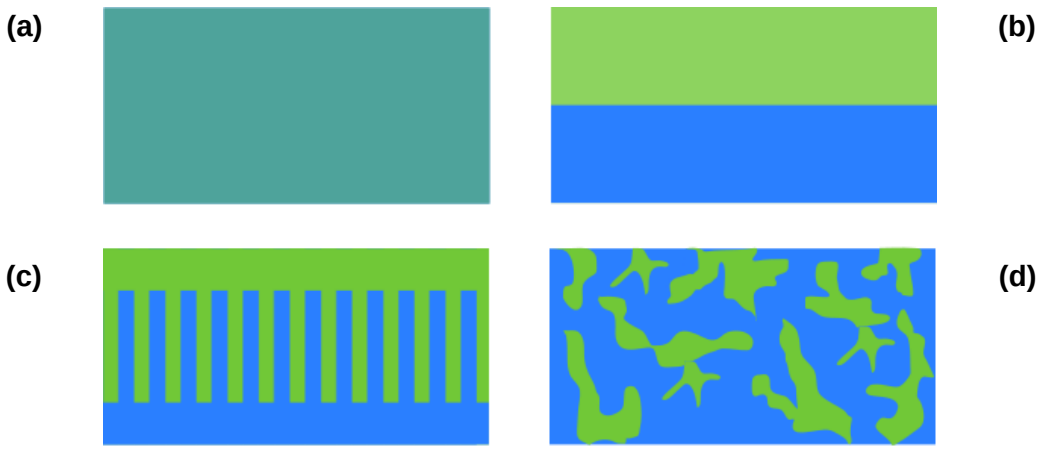

Figure 3 Schematic cross-section of nanomorphology in bulk heterojunction solar cells.
(a) Fine homogeneous donor-acceptor-mixture. (b) Bilayer structure. (c) Ideal arrangement. (d) typical morphology of a solution-processed active layer.

Several methods and processing parameters can be used to improve the phase separation. A post-treatment exposure to solvent vapor or heat leads to a rearrangement of the molecules and therefore to an increased charge carrier mobility. The kind of solvent, the heating temperature and the exposure time are determinative [24]. The nanomorphology also depends on the solvent of the solution that is used to process the active layer [25]. Halogenated aromatic solvents are most commonly used for bulk heterojunction solar cells. A few volume percent of an additive, for example diiodooctane, with a high boiling point and selective solubility in one of the components, can be added to the processing solvent. By delaying the solidification process of either the donor or the acceptor, the other constituent has more time to form ordered structures during the crystallization process. These additives are often used for preparing $PC_{60}BM$ devices [26]. Beside the band gap and the tendency to aggregate, the miscibility and solubility of the components are also an important point. By modifying the chemical structure

of a molecule, these properties can change and therefore ensure a more defined homogeneous and reproducible film [27].

For characterizing a solar cell, the short circuit current, which is the value of the negative photocurrent at zero bias, the open circuit voltage and the fill factor must be measured to determine the power conversion efficiency. Due to the Shockley-Queisser limit a maximum efficiency of 33.3 % should be possible, whereas organic solar cells just reach around 10 %. Götzberger et al. explained that the total costs of a photovoltaic array i.e. on a roof can be reduced by using high efficiency solar cells [28]. Nevertheless, organic solar cells can be very useful in many applications. Beside many convenient features like flexibility, highly reduced thickness (compared to first generation solar cells), light weight and impact resistance endless design possibilities exist. Minor modifications of the chemical structure of the materials used for the active layer leads to a shift of the absorption spectra and therefore to a change of the perceived color of the film [1]. Consequently, the infinite possibility of color variation of organic solar cells in myriad different shapes leads to multifaceted design opportunities and based on the slim design also transparent versions can be fabricated. An application example is pictured in **Figure 4**. It shows a part of the 12-meter-high plant of organic solar cells at the Expo in Milan with the motto “Feeding the Planet, Energy for Life” in 2015 [29].

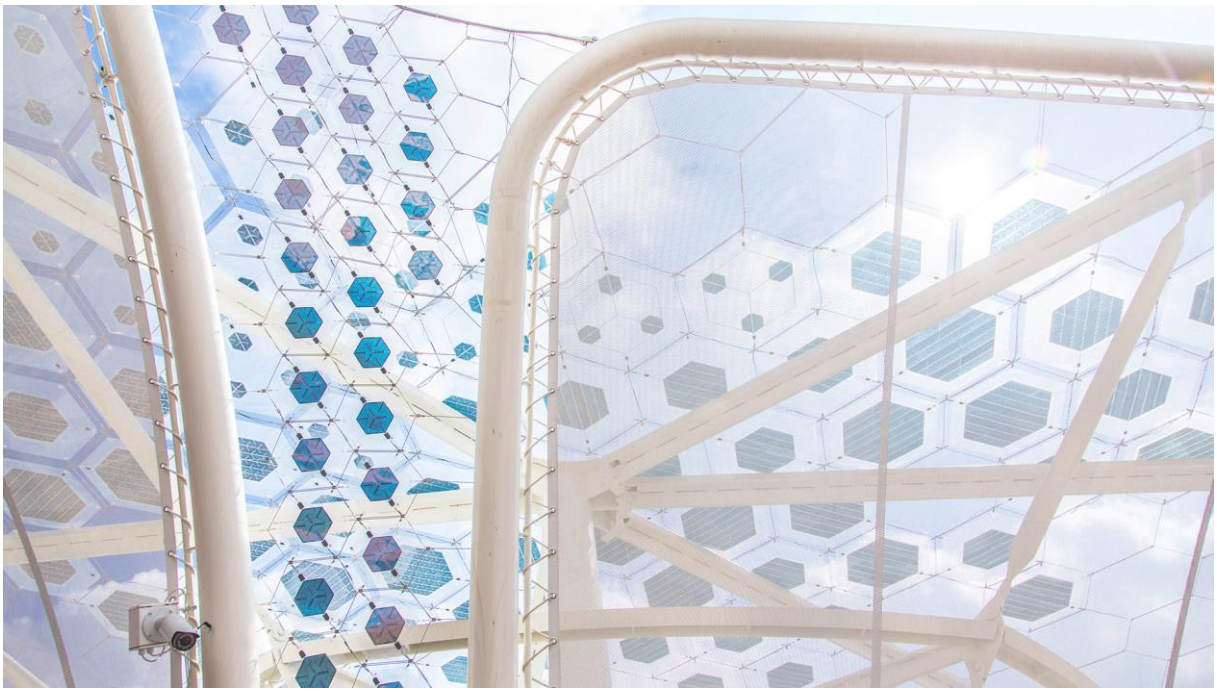

Figure 4 Solar Tree at the German Pavilion of the Universal Exposition 2015 in Milan.

Due to the application from solution, OPVs are printable and can be produced with high throughput. Reduced energy consumption and usage of relatively small amounts of abundant materials are the reasons for low fabrication costs. The production efficiency can be easily increased, due to the possibility of continuous fabrication, which leads to a high output. All these factors make the whole production process scalable and the obtained flexible and light solar cell can be transported to any destination. Another big advantage is that an organic solar cell is truly green.

4. Exprimental

4.1. Materials

Pre-structured ITO substrates were purchased from Xin Yan Technology LTD, Polyethyleneimine and n-Butanol were purchased from Sigma Aldrich. In **Figure 5** the chemical structures of the active layer materials are shown. PBDTTT-EFT (Poly[4,8-bis(5-(2-ethylhexyl)thiophen-2-yl)benzo[1,2-b;4,5-b']dithiophene-2,6-diyl-alt-(4-(2-ethylhexyl)-3-fluoro-thieno[3,4-b]thiophene-)-2-carboxylate-2-6-diyl)]) **(a)** (commonly known as PTB7-Th or PCE10) was purchased from Solarmer, $PC_{60}BM$ (Phenyl-C61-butyricacidmethylester) **(b)** from Solenne, EH-IDTBR (Poly[4,8-bis(5-(2-ethylhexyl)thiophen-2-yl)benzo[1,2-b;4,5-b']di-thiophene-2,6-diyl-alt-(4-(2-ethylhexyl)-3-fluorothieno[3,4-b]thiophene-)-2-carboxylate-2-6-diyl) **(c)** from 1-material and 1,8-diiodooctane from Alfa Aesar.

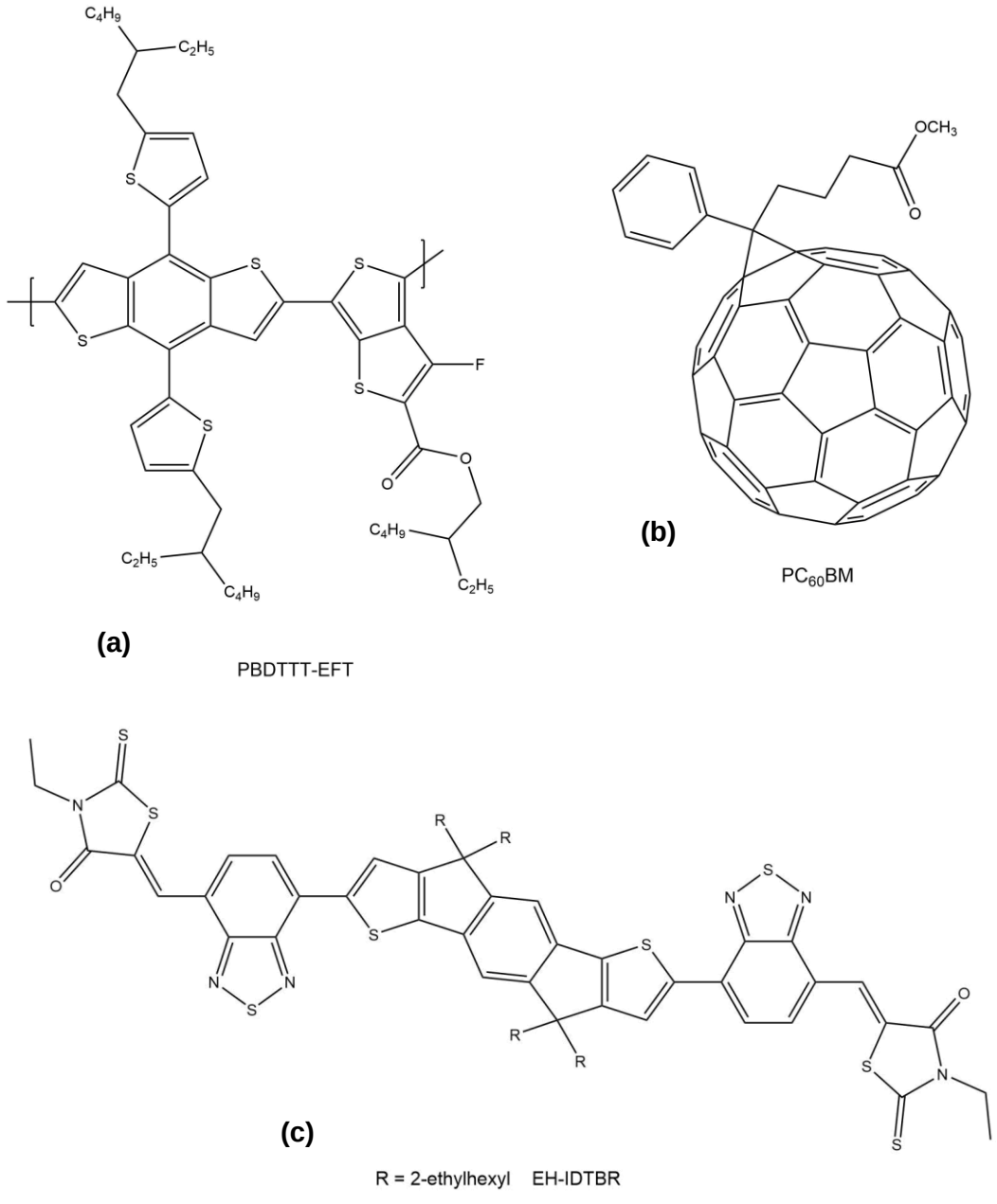

Figure 5 Chemical Structure of the donor and acceptor materials.
(a) PBDTTT-EFT. (b) $PC_{60}BM$. (c) EH-IDTBR.

4.2. Device fabrication and characterization

In **Figure 6** the two possible device configurations are shown. In the standard architecture **(a)** the hole transport layer is applied on the ITO anode, followed by the active layer, the electron transport layer and the cathode on top. The solar cells are fabricated in the inverted structure **(b)** of glass/ITO/PEI/PBDTTT-EFT:EH-IDTBR/MoO_3/Ag, where PEI is used as electron transport layer, followed by the donor-acceptor bulk which functions as the active layer, MoO_3 as the hole transport layer and Ag as the anode.

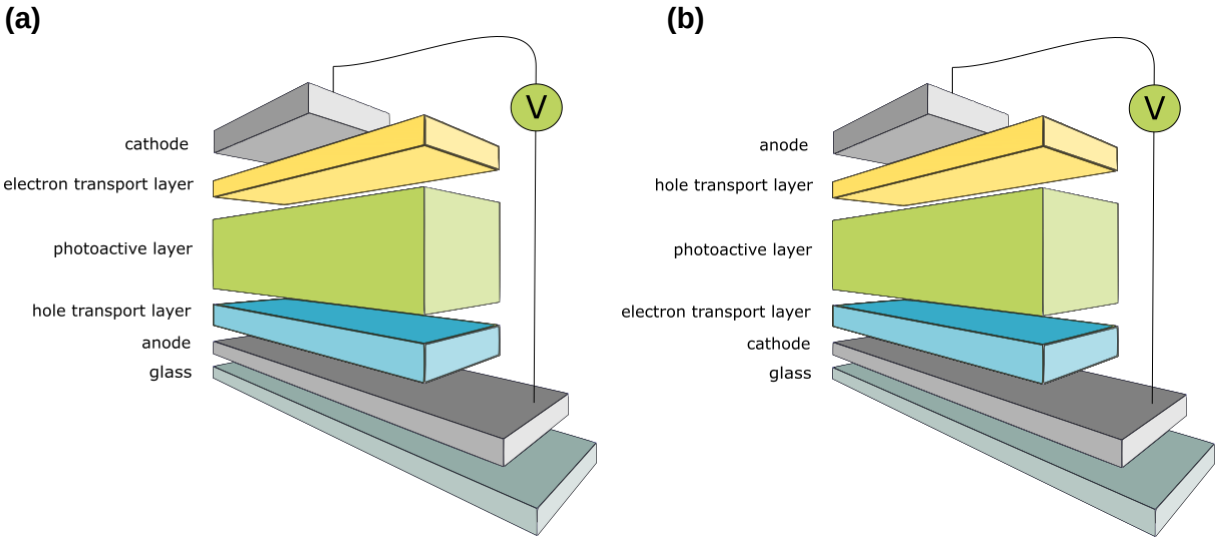

Figure 6 Device architectures of bulk heterojunction solar cells.
(a) Standard design and (b) inverted configuration.

Cleaning of the pre-structured substrates is done with ultra-sonication in acetone at room temperature and isopropanol at 50 °C (15 min each), followed by oxygen plasma treatment (50 W, 5 min). The PEI layer is spin-coated at 5000 rpm for 20 s under ambient conditions from a 0.03 % solution of PEI in *n*-butanol. The pure PBDTTT-EFT layer is applied from a 1 % (10 mg mL^{-1}) solution at 1500 rpm for 2 s followed by an increase in speed to 3000 rpm for 20 s. The layers with D/A 10:1 (1 % PBDTTT-EFT) are spin-coated at 1500 rpm for 2 s followed by an increase to 4000 rpm for 20 s, which leads to a layer thickness of approximately 50 nm. The PBDTTT-EFT:EH-IDTBR (1:1.5) layer is deposited with the same spin-coating parameters from a 0.7 % donor solution (60-70 nm). The PBDTTT-EFT:$PC_{60}BM$ (1:1.5) layer is applied from a 0.7 % solution of PBDTTT-EFT at 2000 rpm for 2 s, followed by 4000 rpm for 20 s (approx. 50 nm). For this solution an additive (2 % DIO) needs to be added to enable the partial separation of the molecules. The deposition of all active layers is done under ambient conditions from a chlorobenzene solution with no further heat annealing. All solutions are stirred over night at 100 °C. The MoO_3 layer (10 nm) and the Ag layer (100 nm) are applied by vacuum vaporization.

The I-V-characteristics are measured under the AM1.5G spectrum (LOT-Quantum Design: Xenon arc lamp with filter) by changing the voltage from -1 to 1 V and detecting the current using a source measuring unit (Keithley 2401 Source Meter). The intensity of the simulated sun is determined with a calibrated silicon solar cell. (Mencke&Tegtmeyer)

For the external quantum efficiency EQE, the current is measured using a potentiostat (Jaissle 1002 T-NC) and a lock-in amplifier (Stanford Research Systems SR830 DSP). As light source a Xenon arc lamp (LOT-Quantum Design) with a holographic grating monochromator (Corner Stone 130 1/8m) is used. The calibration is carried out with a silicon solar cell (Hamamatsu S2281).

4.3. Electroluminescence Quantum Efficiency

In this experiment the electroluminescence quantum efficiency is estimated with a calibrated silicon diode (Hamamatsu S2281). The solar cell is operated at different injection currents. The emitted radiation is detected with a large area and calibrated silicon diode, which is connected to a SMU (Keithley 2401 Source Meter). The measured photocurrent current divided by the injection current through the solar cell gives the electroluminescence quantum efficiency *ELQE*. The calculated values need to be corrected for reflection losses at the substrate air interface and the spectral response of the calibrated silicon diode. With refractive indices $n_{air,660}$ = 1.0002 and $n_{glass,k\text{-}type,546}$ = 1.5131 [35] 12 % can escape the device through the front side of the substrate. The EQE of the calibrated silicon diode is ~ 66 %.

4.4. Photoluminescence and Electroluminescence

The Photoluminescence PL is measured by illuminating the solar cell with a laser (Coherent Obis, excitation wavelength = 488 nm, power = 1 mW). For several experiments, an addition bias voltage is applied to the studied devices (Keithley 2401 Source Meter). The electroluminescence EL is measured by applying a voltage higher than the open circuit voltage on the device. A CCD sensor is used to acquire an image of the luminescent emission (Andor DV420A-OE).

5. Results

In **Figure 7 and 8** the normalized absorption and fluorescence (excitation wavelength = 488 nm) of thin films of the donor and acceptor materials are shown. The photoluminescence curves are all normalized to an input slit width of 500 µm and an exposure time of 1 s. As illustrated in **Figure 7 (a)** the absorption of the PBDTTT-EFT and EH-IDTBR are very similar in the low energy region. The maximum shifts from 1.76 eV (pure donor) to 1.83 eV by increasing the EH-IDTBR content. **Figure 7 (b)** shows that $PC_{60}BM$ absorbs poorly in the visible light range and has its absorption maxima in the ultraviolet range. By increasing the $PC_{60}BM$ content the absorption maximum shifts to 3.67 eV. The absorption spectra of the pure materials are shown in **Figure 8 (a)**. The optical band gap of the semiconductors can be determined by doing a linear regression at the beginning of the absorption spectra, as shown for PBDTTT-EFT in the same figure (red line). The result for the $PC_{60}BM$ film is a relatively high value of 1.98 eV compared to the band gap of EH-IDTBR of 1.64 eV. The optical band gap of $PC_{60}BM$ is the same as reported in the literature [33]. The band gap for the PBDTTT-EFT film was determined as 1.58 eV. The corrected fluorescence curves are shown in **Figure 8 (b)**. Pure EH-IDTBR film shows the strongest fluorescence, which is around 80 times higher than the fluorescence of the pure donor film. The fluorescence of PBDTTT-EFT:EH-IDTBR 10:1 is 30 - 40 times lower compared to the pure donor film. The pure $PC_{60}BM$ film shows the weakest fluorescence. The curve of PBDTTT-EFT:$PC_{60}BM$ 10:1 is lower in the low energy region and overlaps at a value of around 1.85 eV with the curve of PBDTTT-EFT:EH-IDTBR 10:1. The PBDTTT-EFT:EH-IDTBR 1:1.5 signal is at a similar range and decreases again at around 1.85 eV. PBDTTT-EFT:$PC_{60}BM$ 1:1.5 and pure $PC_{60}BM$ give the lowest values that are around 10 times lower than the signal of the 10:1 $PC_{60}BM$ film and around 200 000 times lower compared to the pure EH-IDTBR film.

(a) **(b)**

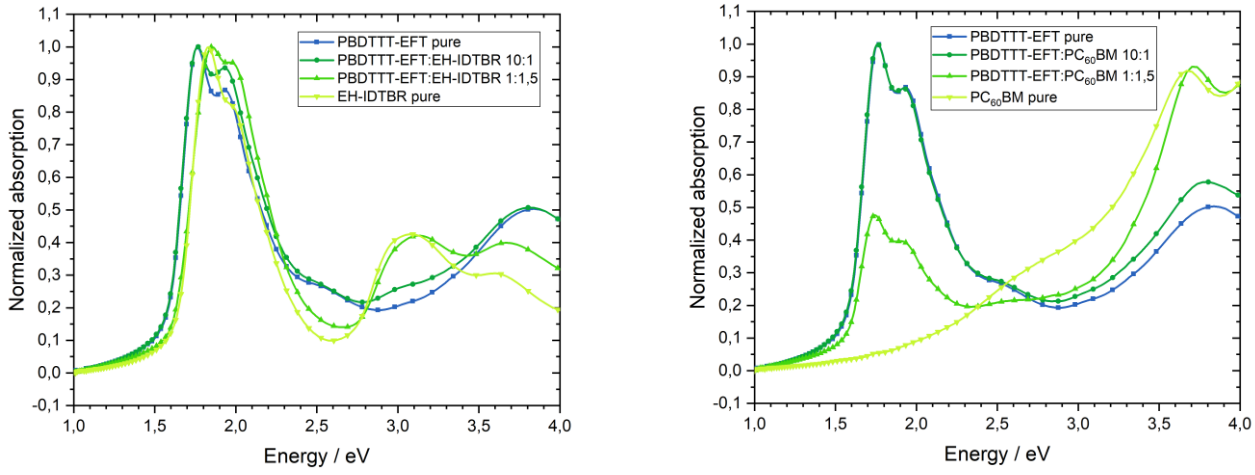

Figure 7 Normalized absorption of PBDTTT-EFT films with EH-IDTBR and $PC_{60}BM$.
(a) Normalized absorption of PBDTTT-EFT and EH-IDTBR pure and with different ratios. (b) Normalized absorption of PBDTTT-EFT and $PC_{60}BM$ pure and with different ratios.

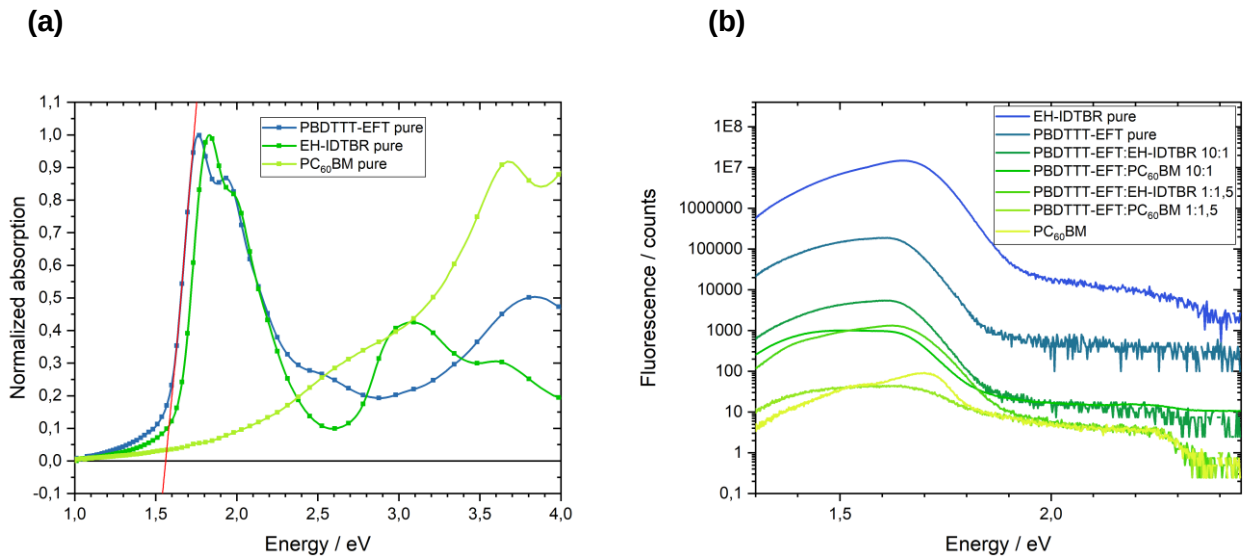

Figure 8 Normalized absorption and fluorescence of PBDTTT-EFT, EH-IDTBR and $PC_{60}BM$ films.
(a) Normalized absorption of pure PBDTTT-EFT, EH-IDTBR and $PC_{60}BM$. (b) Fluorescence of PBDTTT-EFT pure and with different ratios of EH-IDTBR and $PC_{60}BM$.

Table 1 summarizes the photovoltaic parameters and **Figure 9** shows typical current density-voltage characteristics of PBDTTT-EFT solar cells with different ratios of EH-IDTBR and $PC_{60}BM$ and an active area of 15 mm^2 under simulated AM1.5G illumination. The curves were smoothed with Savitzky-Golay method (polynomial order of 2; 20 points). The devices with EH-IDTBR yielded high open circuit voltage (860-1000 mV) and high short circuit current compared to the reference devices with $PC_{60}BM$. The solar cell with a reduced $PC_{60}BM$ content reached a higher open circuit voltage (830 mV) compared to the devices with the usually used D/A ratio (770 mV), which was almost as high as for devices with PBDTTT-EFT:EH-IDBTR 10:1. In general the solar cells with EH-IDTBR in the active layer performed better compared to the devices with $PC_{60}BM$ with the same concentration. EH-IDTBR D/A 1:1.5 has achieved the best short circuit current and open circuit voltage, which leads to an efficiency of 6.7 %. All the devices show quite good dark curves, as shown in **Figure 10**. Without illumination the injection current of the $PC_{60}BM$ solar cells D/A 1:1.5 increases earlier (at a lower voltage value) compared to all other devices.

Table 1 Photovoltaic performance of PBDTTT-EFT:EH-IDTBR and PBDTTT-EFT:$PC_{60}BM$ devices.
J_{SC}… short circuit current, V_{OC}… open circuit voltage, *FF*… fill factor, *PCE*… power conversion efficiency.

	J_{SC} / mA cm^{-2}	V_{OC} / mV	*FF* / %	*PCE* / %
PBDTTT-EFT	0.3	750	30	0.1
PBDTTT-EFT:EH-IDTBR 10:1	5.5	860	30	1.4
PBDTTT-EFT:EH-IDTBR 1:1.5	12.7	1000	53	6.7
PBDTTT-EFT:$PC_{60}BM$ 10:1	4.4	830	26	0.9
PBDTTT-EFT:$PC_{60}BM$ 1:1.5	9.8	770	63	4.8

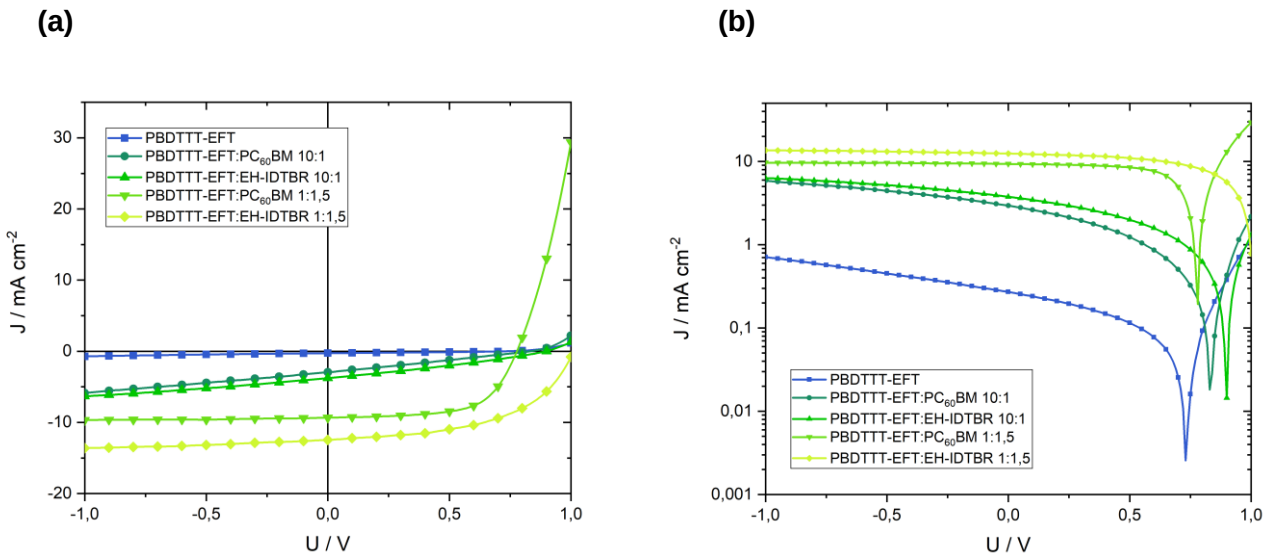

Figure 9 *I-V*-characteristics of PBDTTT-EFT devices with EH-IDTBR and $PC_{60}BM$ under simulated illumination.
On a linear scale (a) and on a logarithmic scale (b).

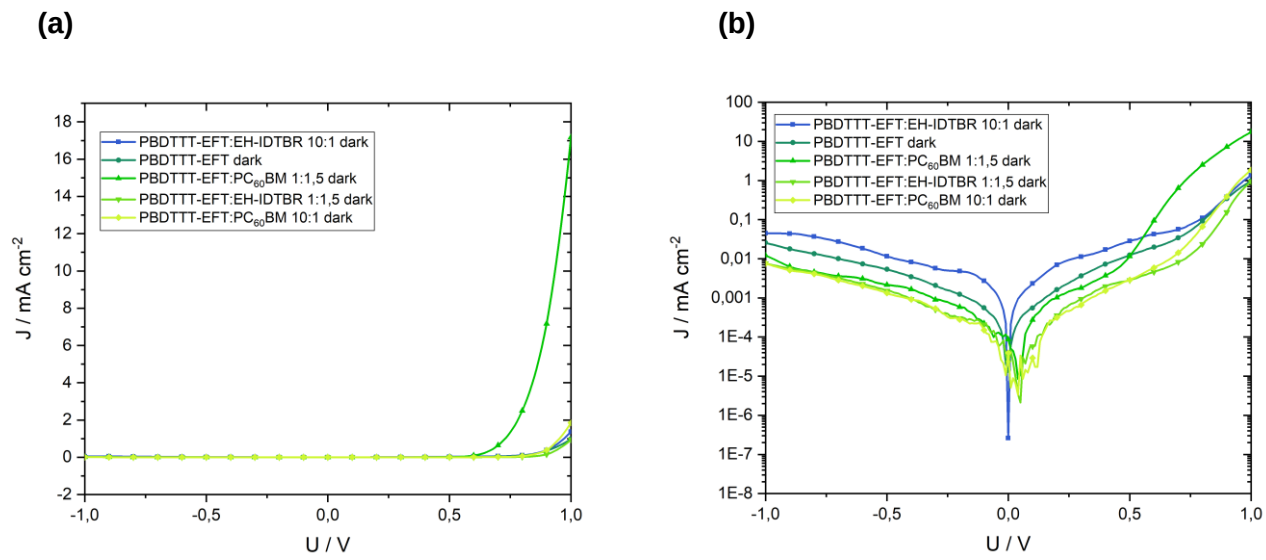

Figure 10 Dark curves of PBDTTT-EFT:EH-IDTBR and PBDTTT-EFT:$PC_{60}BM$ devices.
On a linear scale (a) and on a logarithmic scale (b).

Figure 11 shows the external quantum efficiency of the fabricated devices with different donor/acceptor ratio. The optimized EH-IDBTR solar cell (1:1.5) reaches a value up to 69 % at 670 nm. The device with fullerene acceptor shows a lower *EQE* with a maximum of 51 % at 710 nm. In **Figure 11 (b)** the same EQE spectra are plotted on a log-scale and versus photon energy. Compared to the EQE spectrum of the PBDTTT-EFT device, all solar cells containing an acceptor show EQEs extending further to the infrared region. PBDTTT-EFT mixed with PCBM show higher EQEs in the low energy region of the spectra compared to solar cells containing EH-IDTBR.

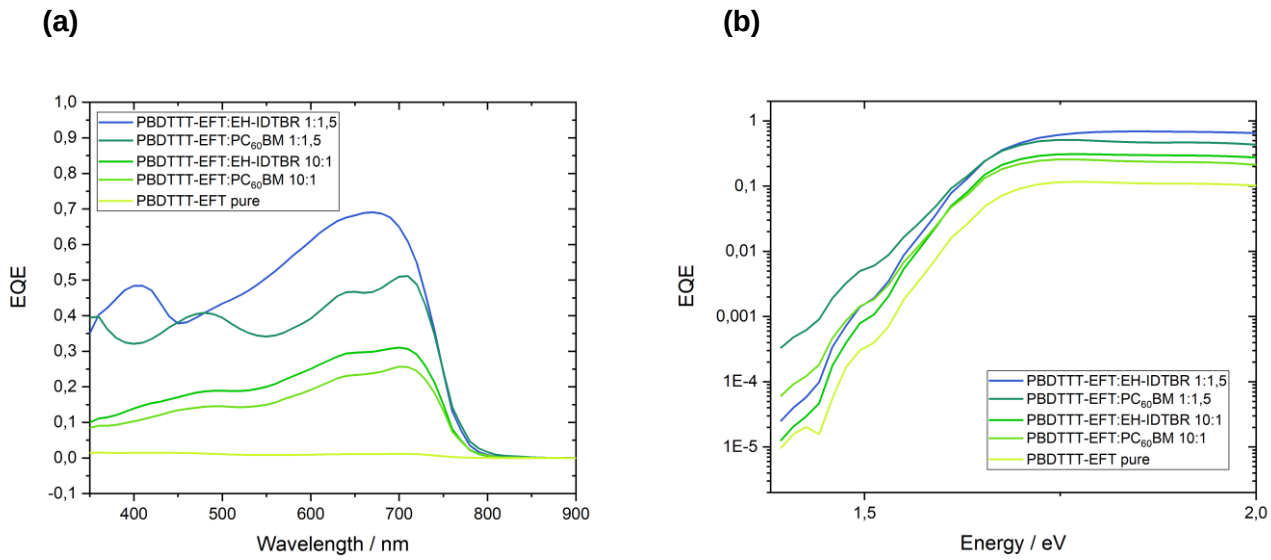

Figure 11 *EQE* of PBDTTT-EFT:EH-IDTBR and PBDTTT-EFT:PC_{60}BM devices.
As a function of wavelength on a linear scale (a) and as a function of the energy of a photon on a logarithmic scale (b).

The absorption spectra and the *EQE* of devices with ideal D/A ratio are compared in **Figure 12 (a)**. The spectra overlap nicely. Interference effects broaden the EQE spectra and induce stronger photon absorption in the 400-500 nm range of the spectra. In **Figure 12 (b)** the electroluminescence quantum efficiencies of the prepared devices measured under different injection currents are shown. By increasing the PC_{60}BM content, much higher current inputs are needed to detect radiative recombination. In the entire investigated current range the *ELQE* of the pure device and the devices with non-fullerene acceptor is much higher compared to the fullerene based solar cells. At low injection currents the PBDTTT-EFT:EH-IDTBR 1:1.5 solar cell exhibits the highest ELQE. At larger injection currents the device based on a pristine PBDTTT-EFT absorber/emitter layer shows the highest ELQE. PBDTTT-EFT:PC_{60}BM 10:1 shows a lower ELQE compared to pristine polymer or EH-IDTBR based devices. PBDTTT-EFT:PC_{60}BM 1:1.5 gives the weakest electroluminescence. The presented *ELQE*s should be considered as approximate values. Especially at high injection current – heating of the devices leads to fluctuations in the device output.

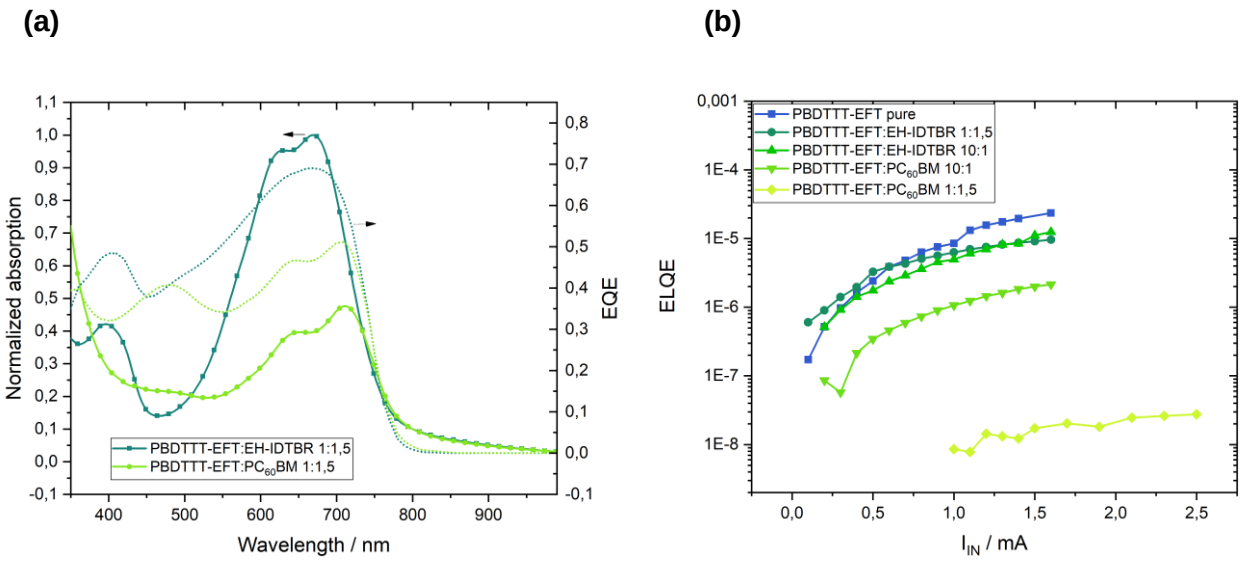

Figure 12 (a) *EQE* and normalized absorption of PBDTTT-EFT devices with EH-IDTBR and $PC_{60}BM$ D/A 1:1.5. (b) *ELQE* of PBDTTT-EFT devices with EH-IDTBR and $PC_{60}BM$.
EQE as a function of wavelength (solid lines) alongside normalized thin film absorption spectra (dotted lines). *ELQE* as a function of applied current.

In **Figure 13** and **Figure 14** the dependence of the photoluminescence on a voltage applied to the investigated device is illustrated. The curves are all corrected to a monochromator input slit width of 1000 µm and an exposure time of 1 s. The electroluminescence curves are smoothed with Savitzky-Golay method (polynomial order of 2; 100 points). For comparison also the electroluminescence is plotted in the Figures. For the pure donor device (**Figure 13 (a)**, **(b)**) there is virtually no impact on the photoluminescence upon applying different voltages. Upon adding acceptor molecules to the donor material, the radiative recombination in the devices is sensitive to an external voltage. This effect occurs for an ideal D/A ratio (1:1.5) (**Figure 13 (c)** and **Figure 14 (a)**) and is even stronger at lower acceptor concentrations (**Figure 13 (e)** and **Figure 14 (c)**). Under short circuit conditions, the photoluminescence is smallest and increases upon increasing the applied bias. Furthermore, a change in the shape and a red shift of the electroluminescence compared to the photoluminescence is observed for solar cells containing EH-IDTBR (**Figure 13 (d)**, **(f)**). The effect is more pronounced for $PC_{60}BM$ based solar cells (**Figure 14 (b)**, **(d)**).

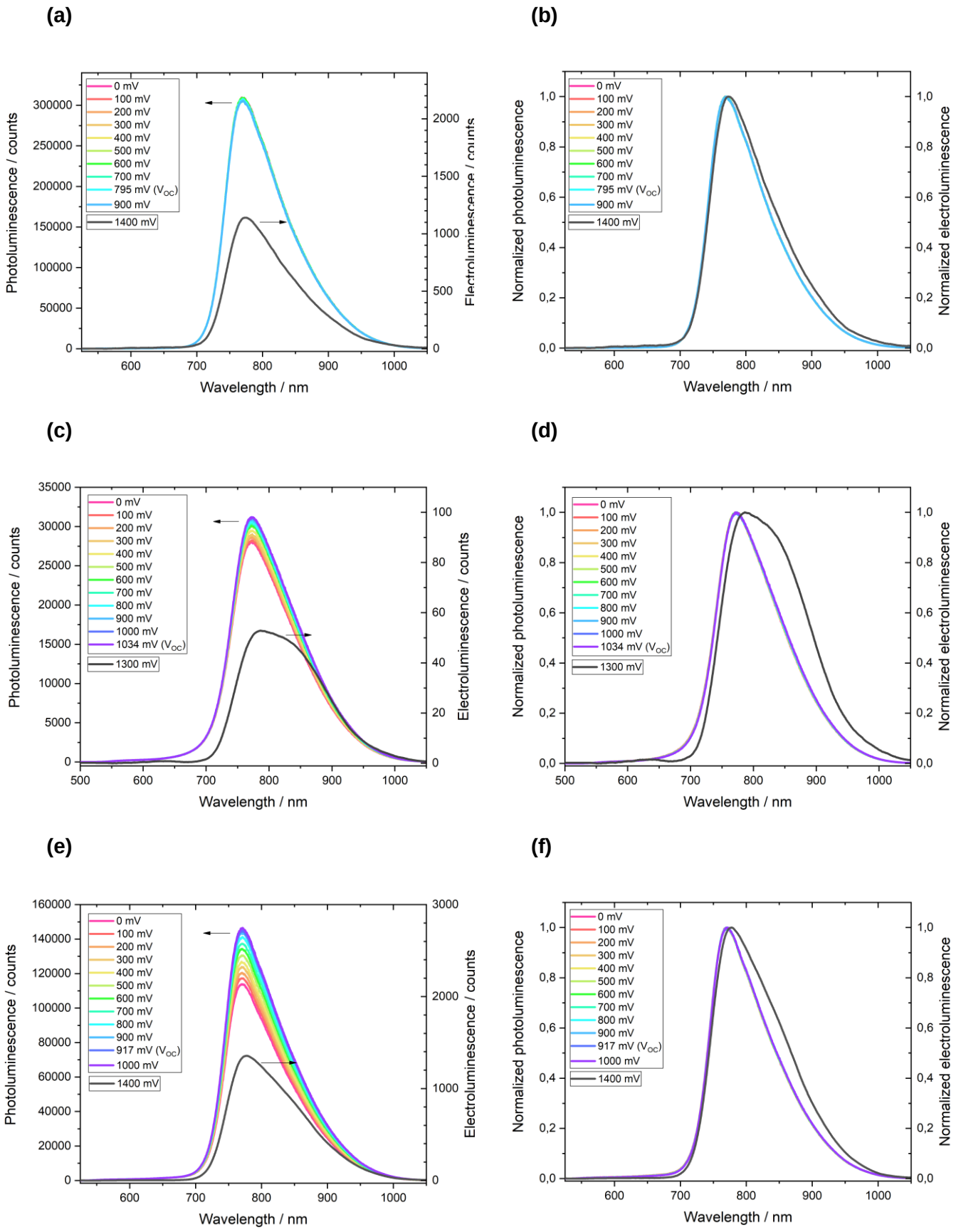

Figure 13 Photoluminescence and Electroluminescence as a function of wavelength.
PL and EL of a pristine PBDTTT-EFT device, originally (a) and normalized (b).
PL and EL of a PBDTTT-EFT:EH-IDTBR device D/A 1:1.5, originally (c) and normalized (d).
PL and EL of a PBDTTT-EFT:EH-IDTBR device D/A 10:1, originally (e) and normalized (f).

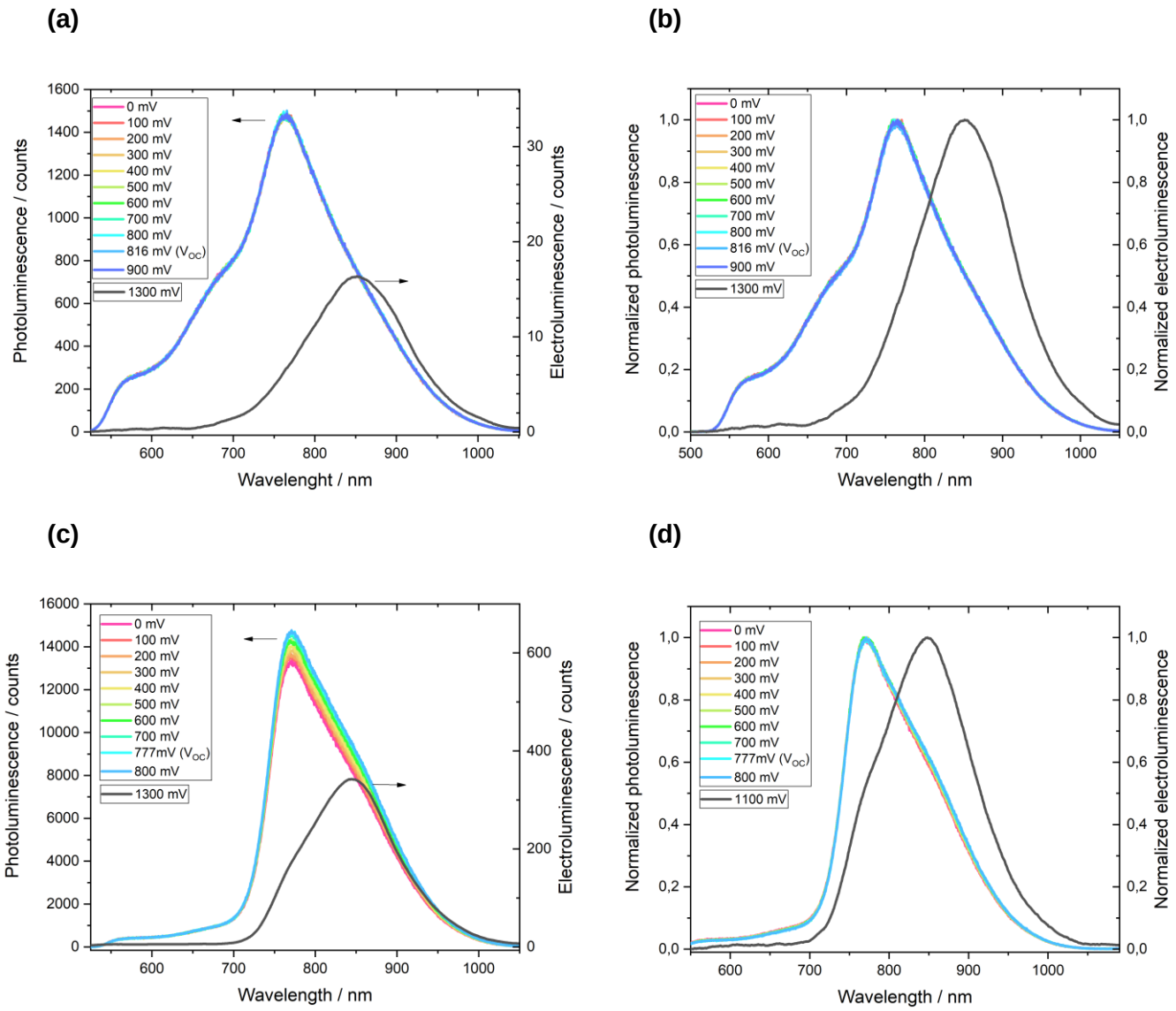

Figure 14 Photoluminescence and Electroluminescence as a function of wavelength.
PL and EL of a PBDTTT-EFT:$PC_{60}BM$ device D/A 1:1.5, originally (a) and normalized (b).
PL and EL of a PBDTTT-EFT:$PC_{60}BM$ device D/A 10:1, originally (c) and normalized (d).

6. Discussion

The performed experiments clearly reveal the advantage of the investigated non-fullerene acceptor EH-IDTBR over the standard acceptor $PC_{60}BM$. The non-fullerene acceptor shows a strong absorption in the visible and near infrared region of the solar spectrum leading to a significant contribution to photocurrent of the photovoltaic devices. In contrast, $PC_{60}BM$ absorbs only in the high-energy region and is a less efficient absorber for solar radiation.

Optimized PBDTTT-EFT:EH-IDTBR solar cells show a higher open circuit voltage compared to devices with the same donor and $PC_{60}BM$ as acceptor. This observation is also reflected in the fact that the position of the charge transfer state is different in the two donor acceptor blends. For devices with fullerene acceptor, the low energy tail of the external quantum efficiency is more pronounced compared to the solar cell with the optimized concentration of EH-IDTBR. This finding is also supported by the photoluminescence and electroluminescence experiments. For devices with a pristine PBDTTT-EFT active layer, the photoluminescence and the electroluminescence spectra are essentially identical. Upon adding $PC_{60}BM$ the PL and the EL spectra recorded on solar cells appear at different positions. EL shifts about 0.15 eV with respect to the PL maximum. When EH-IDTBR is added to the donor polymer, the shift between the photoluminescence and the electroluminescence is much smaller. The EL spectra do show an additional low-energy shoulder.

The EQE, photoluminescence and electroluminescence data suggest that the charge-transfer state formed in the donor-acceptor blends have different energetics. In EL experiments, injected charges recombine through the lowest lying energetic states. In the investigated donor acceptor blends this is the charge transfer state.

Also the electroluminescence quantum yield measurements support the observation of higher open circuit voltages for solar cells with non-fullerene acceptors. It is well excepted that the open circuit voltage depends on the radiative recombination quantum yield (Shockely-Queisser Limit). Higher yields lead to higher open circuit voltages. For all studied devices the quantum yields are still quite small – suggesting that the open circuit voltages losses are still substantial even in non-fullerene acceptor based solar cells.

The observation of a voltage-dependent photoluminescence is very interesting and is reported for the first time for organic solar cells with non-fullerene acceptors. In pristine PBDTTT-EFT devices there is nearly no impact on the photoluminescence when applying a bias. In devices with high fullerene content, the effect of an applied voltage is very small. The observed emission is coming from photo-excited excitons, which do not undergo charge separation. In the devices with non-fullerene acceptors the voltage dependence can even be observed at high acceptor loadings. The devices with the strongest photoluminescence change also give the best values for the open circuit voltage (830 – 1000 mV). The experiment shows that the emission originates at least partially for photo-induced charge carriers, which can recombine radiatively in the semiconductor layer. Additional experiments on a detailed modelling of the voltage dependent photoluminescence are required to derive more quantitative results. All the performed experiments support the current understanding that using non-fullerene acceptors is a very promising approach to increase the power conversion efficiency of organic solar cells.

7. Conclusion

In this thesis, the properties of EH-IDTBR and $PC_{60}BM$ are investigated as acceptors in organic solar cells. The optical properties of thin films and opto-electronic properties of photovoltaic devices are studied in detail. The EH-IDTBR-based devices reach a higher open circuit voltage as well as higher short circuit currents compared to fullerene-bases devices. With the measurement of the external quantum efficiency and the photo- and the electroluminescence, the presence of a charge transfer state in fullerene devices is shown. For EH-IDTBR devices the charge transfer complex is shifted to higher energies. The radiative recombination is found to be more efficient in EH-IDTBR-based solar cells. These findings explain the high open circuit voltage observed for the solar cells containing EH-IDTBR. All experimental results demonstrate a huge potential for reaching even better power conversion efficiency when non-fullerene acceptors like EH-IDTBR are used.

8. References

[1] C. Brabec, V. Dyakonov, and U. Scherf, *Organic Photovoltaics: Materials, Device Physics and Manufacturing Technologies*. 2009.

[2] A. F. Eftaiha, J. Sun, G. Hill, and G. C. Welch, “acceptors for solution processed bulk heterojunction solar cells,” pp. 1201–1213, 2014.

[3] C. Deibe, T. Strobe, and V. Dyakonov, “Role of the charge transfer state in organic donor-acceptor solar cells,” *Adv. Mater.*, vol. 22, no. 37, pp. 4097–4111, 2010.

[4] A. Luque and S. Hegedus, *Handbook of Photovoltaic Science and Engineering*. 2011.

[5] C. E. Fritts, “On a new form of selenium cell and some electrical discoveries made by its use,” *Am. J. Sci.*, vol. s3-26, no. 156, pp. 465–472, 1883.

[6] A. Einstein, “On a Heuristic Viewpoint Concerning the Production and Transformation of Light,” *Annalen der Physik*, vol. 17, no. 6. pp. 132–148, 1905.

[7] M. Volmer, “Die verschiedenen lichtelektrischen Erscheinungen am Anthracen, ihre Beziehungen zueinander, zur Fluoreszenz und Dianthracenbildung,” *Ann. Phys.*, vol. 345, no. 4, pp. 775–796, 1913.

[8] P. M. Borsenberger, “Organic Photoreceptors for Xerography.” 1993.

[9] H. Inokuchi, “The discovery of organic semiconductors. Its light and shadow,” *Org. Electron. physics, Mater. Appl.*, vol. 7, no. 2, pp. 62–76, 2006.

[10] H. Gerischer, M. E. Michel-Beyerle, F. Rebentrost, and H. Tributsch, “Sensitization of charge injection into semiconductors with large band gap,” *Electrochim. Acta*, vol. 13, no. 6, pp. 1509–1515, 1968.

[11] C. W. Tang and A. C. Albrecht, “Photovoltaic effects of metal-chlorophyll-a-metal sandwich cells,” *J. Chem. Phys.*, vol. 2139, no. 1975, pp. 2139–2149, 1975.

[12] H. Shirakawa, E. Louis, A. MacDiarmid, C. K. Chiang, and A. J. Heeger, “Synthesis of Electrically Conducting Organic Polymers,” *Polymer (Guildf).*, vol. 36, no. 578, pp. 578–580, 1977.

[13] M. C. Scharber and N. S. Sariciftci, “Bulk Heterojunction Organic Solar Cells: Working Principles and Power Conversion Efficiencies,” in *Nanostructured Materials for Type III Photovoltaics*, Royal Society of Chemistry, 2018, pp. 33–68.

[14] C. W. Tang, “Two-layer organic photovoltaic cell,” *Appl. Phys. Lett.*, vol. 48, no. 2, pp. 183–185, 1986.

[15] N. Sariciftci, L. Smilowitz, A. J. Heeger, and F. Wudl, “Photoinduced Electron Transfer from a Conducting Polymer to Buckminsterfullerene.,” *Science (80-.).*, vol. 258, pp. 1474–1476, 1992.

[16] P. Würfel and U. Würfel, *Physics of Solar Cells: From Basic Principles to Advanced Concepts*. Wiley-VCH, 2016.

[17] W. Shockley and H. J. Queisser, “Detailed balance limit of efficiency of p-n junction solar cells,” *J. Appl. Phys.*, vol. 32, no. 3, pp. 510–519, 1961.

[18] H. Bässler and A. Köhler, “Charge Transport in Organic Semiconductors,” *Top Curr Chem*, vol. 312, no. 1, pp. 1–66, 2012.

[19] S. Foster *et al.*, “Electron collection as a limit to polymer:PCBM solar cell efficiency: Effect of blend microstructure on carrier mobility and device performance in PTB7:PCBM,” *Adv. Energy Mater.*, vol. 4, no. 14, pp. 1–12, 2014.

[20] M. C. Scharber and N. S. Sariciftci, “Efficiency of bulk-heterojunction organic solar cells,” *Prog. Polym. Sci.*, vol. 38, no. 12, pp. 1929–1940, 2013.

[21] M. C. Scharber *et al.*, “Design rules for donors in bulk-heterojunction solar cells - Towards 10 % energy-conversion efficiency,” *Adv. Mater.*, vol. 18, no. 6, pp. 789–794,

2006.

[22] O. V. Mikhnenko, H. Azimi, M. Scharber, M. Morana, P. W. M. Blom, and M. A. Loi, “Exciton diffusion length in narrow bandgap polymers,” *Energy Environ. Sci.*, vol. 5, no. 5, pp. 6960–6965, 2012.

[23] P. Morvillo, E. Bobeico, S. Esposito, and R. Diana, “Effect of the active layer thickness on the device performance of polymer solar cells having [60]PCBM and [70]PCBM as electron acceptor,” *Energy Procedia*, vol. 31, pp. 69–73, 2011.

[24] G. Li *et al.*, “High-efficiency solution processable polymer photovoltaic cells by self-organization of polymer blends,” *Nat. Mater.*, vol. 4, no. 11, pp. 864–868, 2005.

[25] S. E. Shaheen, C. J. Brabec, N. S. Sariciftci, F. Padinger, T. Fromherz, and J. C. Hummelen, “2.5% Efficient Organic Plastic Solar Cells,” *Appl. Phys. Lett.*, vol. 78, no. 6, pp. 841–843, 2001.

[26] J. Peet *et al.*, “Efficiency enhancement in low-bandgap polymer solar cells by processing with alkane dithiols,” *Nat. Mater.*, vol. 6, no. 7, pp. 497–500, 2007.

[27] Z. B. Henson, K. Müllen, and G. C. Bazan, “Design strategies for organic semiconductors beyond the molecular formula,” *Nat. Chem.*, vol. 4, no. 9, pp. 699–704, 2012.

[28] A. Goetzberger, J. Knobloch, and B. Voß, *Crystalline Silicon Solar Cells*. John Wiley & Sons, Ltd, 2014.

[29] “Solar Trees – Stories Merck Global.” [Online]. Available: https://www.merckgroup.com/en/stories/organic_photovoltaics_generating_power_and-creating_shade.html. [Accessed: 27-Sep-2018].

[30] “Key World Energy Statistics,” 2017.

[31] German Advisory Council on Global Change, *World in Transition – Towards Sustainable Energy Systems*. 2003.

[32] D. R. Lide, “CRC Handbook of Chemistry and Physics, 84th Edition, 2003-2004,” *Handb. Chem. Phys.*, vol. 53, p. 2616, 2003.

[33] W. C. H. Choy, *Organic Solar Cells: Materials and Device Physics*. 2013.

“The roots of education are bitter, but the fruit is sweet.” – Aristotle